Investigation of the Large-Scale and Statistical Properties of Richtmyer-Meshkov Instability-Induced Mixing

Presented at:

9th International Workshop on the Physics of Compressible Turbulent Mixing
Cambridge, UK

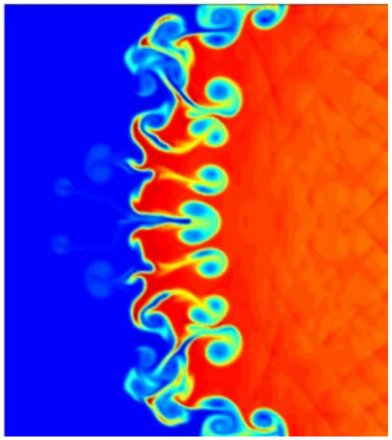

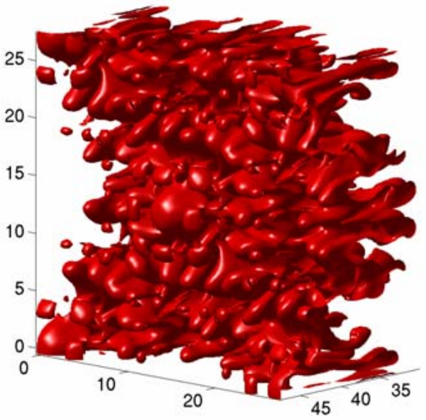

[1]Oleg Schilling, [2]Marco Latini, [3]Wai-Sun Don

[1]Lawrence Livermore National Laboratory, [2]California Institute of Technology, [3]Brown University

21 July 2004

This work was performed under the auspices of the U.S. Department of Energy by the University of California Lawrence Livermore National Laboratory under Contract No. W-7405-Eng-48.

Lawrence Livermore National Laboratory, P.O. Box 808, Livermore, CA 94551-0808

UCRL-PRES-205225

The purpose of this research is to numerically study the physics of single- and multi-mode Richtmyer-Meshkov instability and mixing with reshock in 2D and 3D

- **Apply a high-resolution, Eulerian, shock-capturing reconstruction-evolution method to Richtmyer-Meshkov instability with reshock**
- **Compare to experimental data (Collins-Jacobs and Vetter-Sturtevant); extend simulations/analysis to longer *t***
- **Study <u>dynamics and structure</u>, including mixing: time-evolution of global mixing and flow statistics, spectra, *terms in evolution equations***
- **Investigate effects of <u>reshock</u>**
- **Examine <u>differences between 2D and 3D mixing</u>**

The topics of this investigation are essential to the development/validation of subgrid-scale and turbulent mixing models for complex shock-induced flows

Simulations were performed using the weighted essentially non-oscillatory (WENO) method

- **Euler equations solved using local Lax-Friedrichs flux-split finite-difference reconstructions**
- **Convex linear combination of all possible polynomial interpolations taken to achieve ENO property**
  - **High-order non-oscillatory solutions obtained using nonlinearly-weighted set of stencils that avoid crossing discontinuities**
  - **Local characteristic decomposition for flux-splitting**
- **3rd-order TVD Runge-Kutta method for time-evolution**
- **Notable features of code**
  - **3rd-, 5th-, 7th-, 9th-, or 11th-order WENO reconstruction**
  - **Adaptive domain method increases number of grid points dynamically**
  - **Interface tracked by mass fraction**
  - **Multi-resolution hybridization with high-order central-difference schemes**

A model of the *Ma* = 1.21 Collins-Jacobs air(acetone)/SF_6 shock tube experiment was simulated with reshock for initial code validation

WENO 5 Simulation Parameters		
Domain Size	8.9 cm x 75 cm	
Grid spacing	$\Delta x = \Delta y = 0.02$ cm	
Initial perturbation properties	Amplitude a_0	0.183 cm
	Wavelength λ	5.9 cm
	Diffusion thickness	0.5 cm
Air(acetone)-SF_6 Properties	Pre-shock Atwood number A^-	0.604
	Adiabatic exponent γ	1.24815

Density at *t* = 5 ms

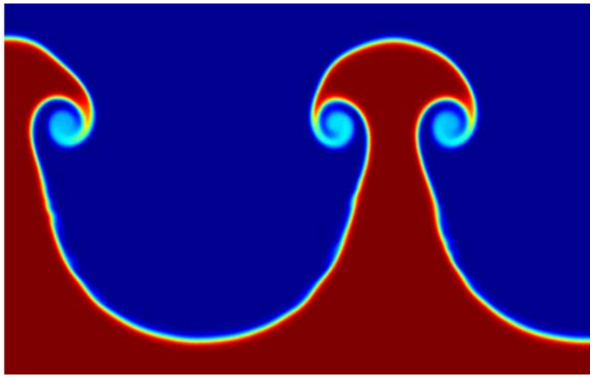

Vorticity at *t* = 5 ms

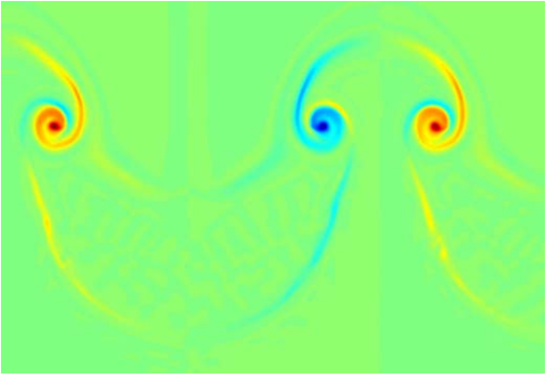

Simulation and experimental density are in good agreement initially; lack of rarefaction to slow interface causes reflected shock to interact with interface ~ 1 ms sooner

After Reshock

PLIF images from Collins and Jacobs

t = 2 .502 ms **t = 4.009 ms** **t = 5.015 ms** **t = 7.005 ms** **t = 7.781 ms**

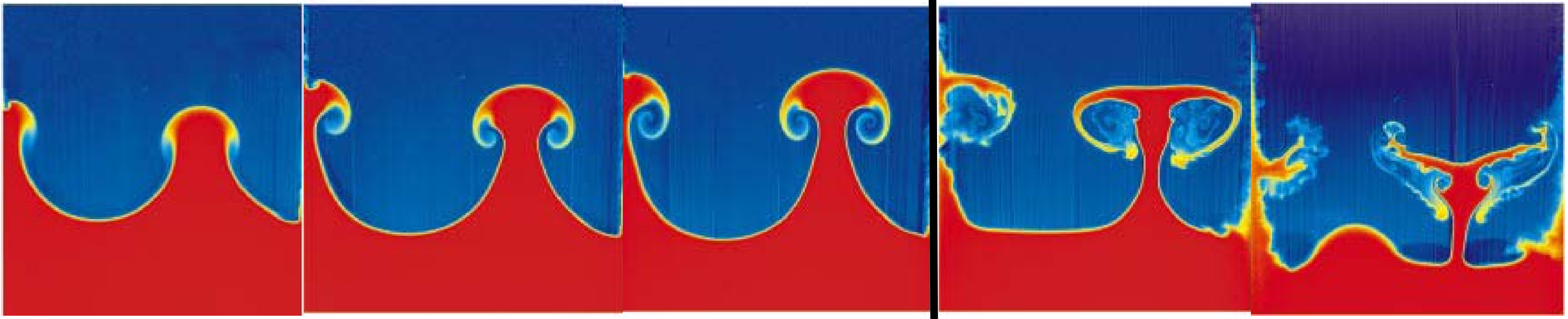

t = 2.5 ms **t = 4 ms** **t = 5 ms** **t = 6.47 ms** **t = 6.78 ms**

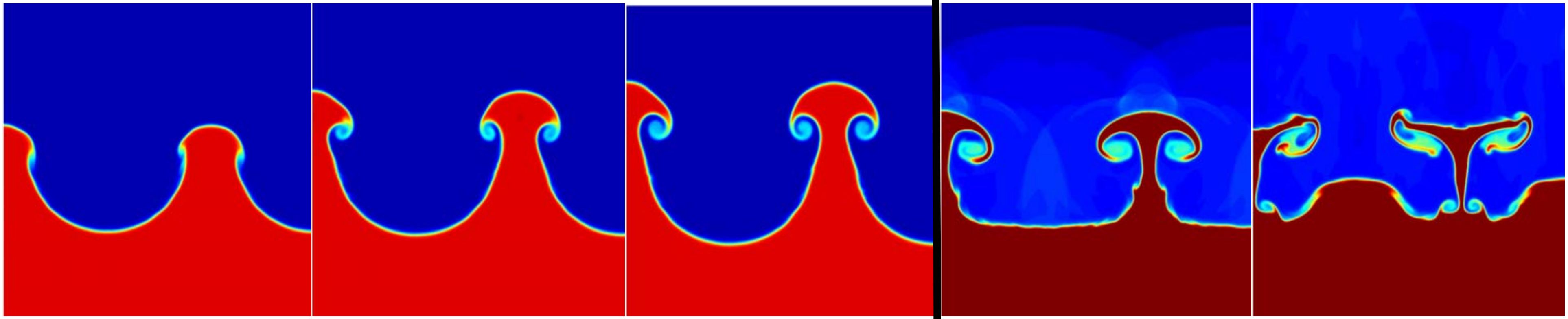

5th-order WENO simulations

Nonlinear perturbation series extended via Padé approximants can capture nonlinear mixing layer width evolution prior to reshock

- **Zhang and Sohn (Padé) (1997):**

$$\frac{da}{dt}=\frac{v_0}{1+k\,a_0\,\tau+\max\left[0,k^2a_0^2-\left(A^+\right)^2+\frac{1}{2}\right]\tau^2}$$

- **Vandenboomgaerde et al. (2002):**

$$a(t)=a_0+\frac{1}{k}\sum_{n=0}^{N}P_{2n+1}(A^+)\left(k\,a_0\,\sigma t\right)^{2n+1}$$

$$\sigma=\frac{k[v]}{2}\left(A^+ +\frac{A^-}{1-[v]/v_s}\right)$$

- **Sadot et al. (1998):**

$$\frac{da_{b,s}}{dt}=\frac{v_0\left(1+\tau\right)}{1+\left(1\pm A^+\right)\tau+\frac{3}{2}\frac{1\pm A^+}{1+A^+}\tau^2}$$

$$\frac{da}{dt}=\frac{1}{2}\left(\frac{da_b}{dt}+\frac{da_b}{dt}\right)$$

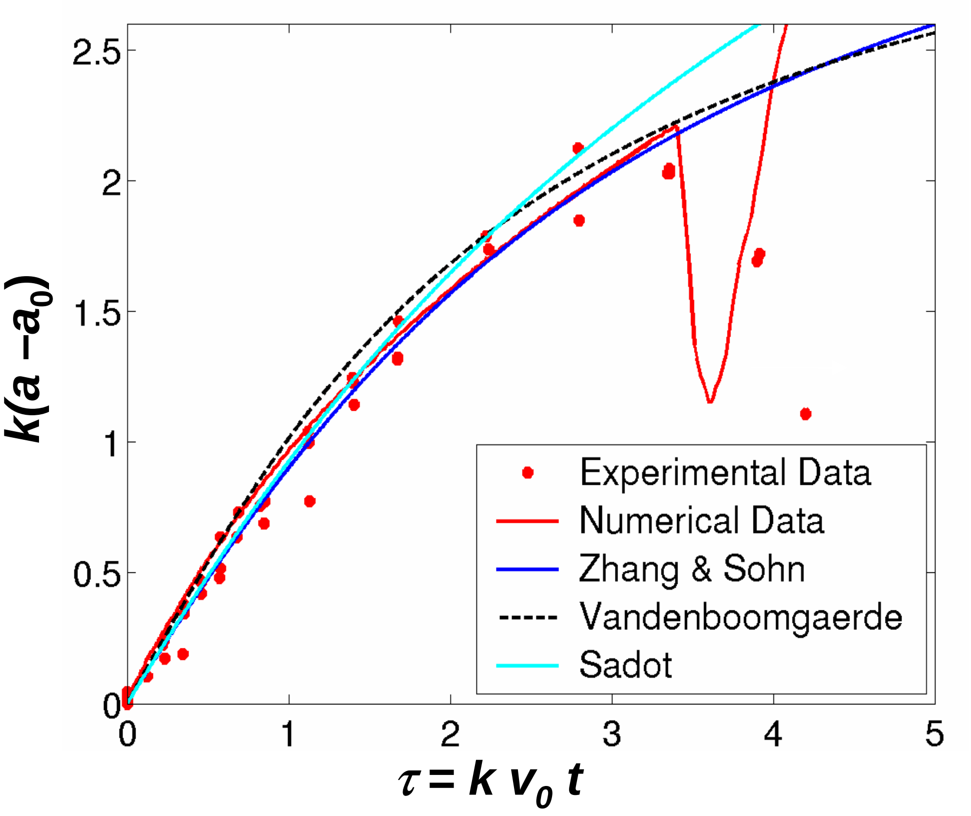

- **Experimental data in best agreement with Sadot model**
- **Simulation data in best agreement with Zhang-Sohn (Padé) model**

Ma = 1.5 air/SF$_6$ Vetter Sturtevant experiment with wire mesh and membrane is modeled using a two-mode initial perturbation

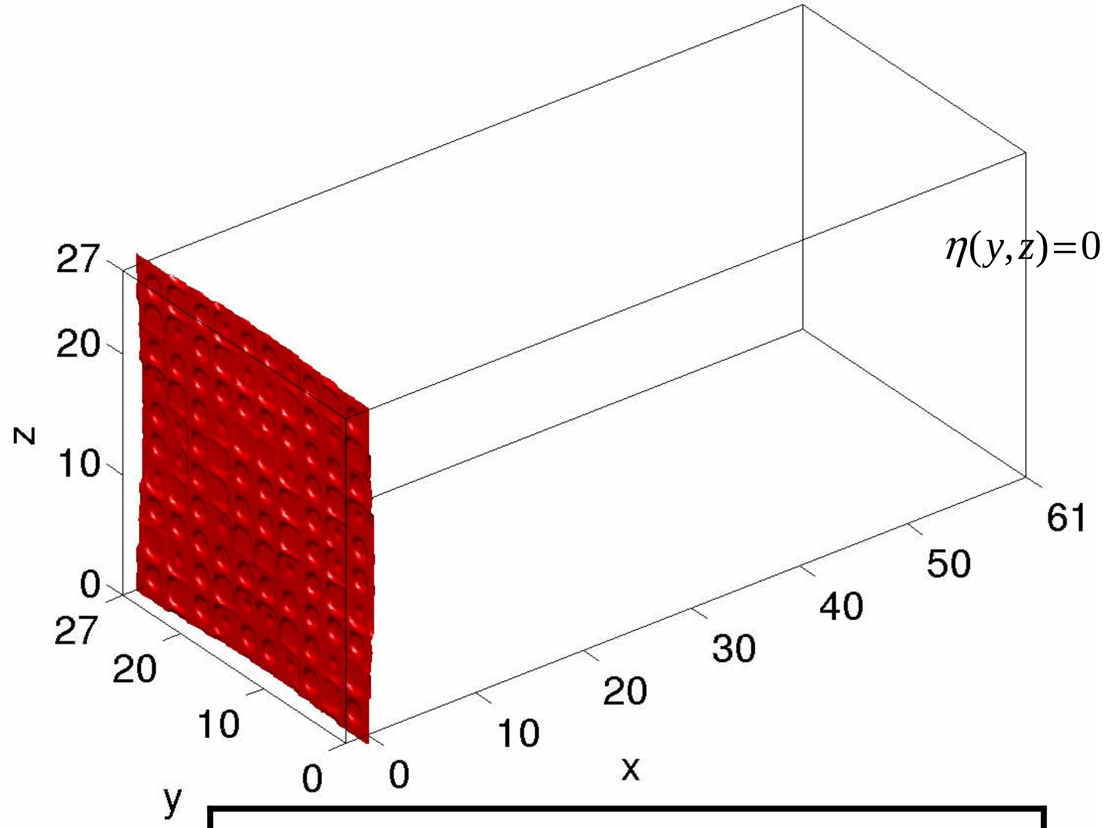

Initial perturbation model:

$$\eta(y,z)=0.27\left[\underbrace{|\sin(10\pi y)||\sin(10\pi z)|}_{\text{models membrane pushed through mesh}}-\underbrace{\cos(2\pi y)\cos(2\pi z)}_{\text{models distortion of mesh}}\right]$$

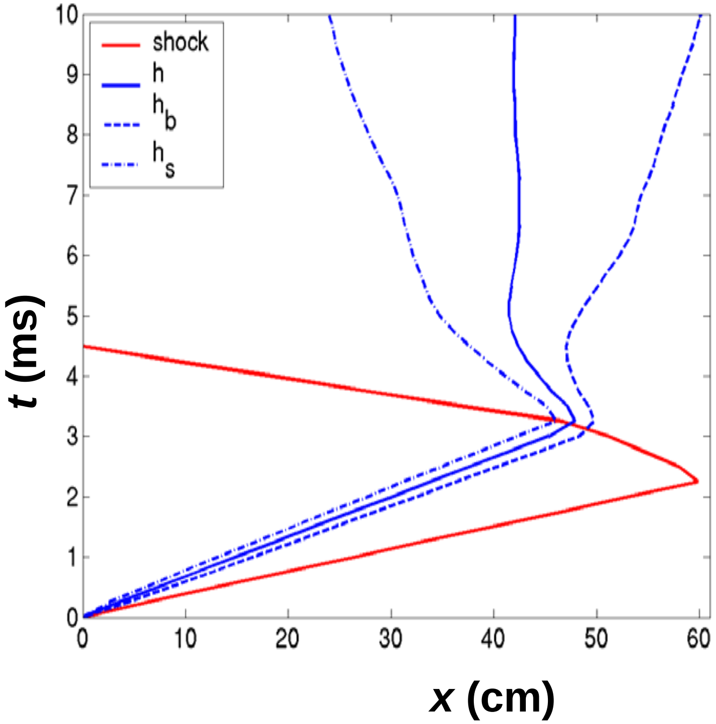

Simulation Resolutions and Orders		
2D WENO 5	**1300 × 540**	
3D WENO 5	**257 × 129^2**	**401 × 257^2**
3D WENO 9	**257 × 129^2**	

Animations

- **Time-evolution of mass fraction isosurface in 3D**
- **Time-evolution of mass fraction in 2D**

Mass fraction isosurface from high-order WENO simulation shows detailed structure before and following reshock

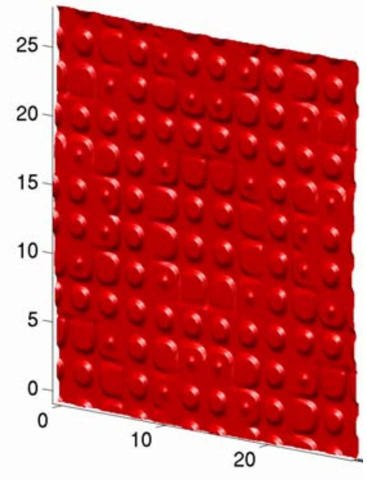

t **= 0 ms**

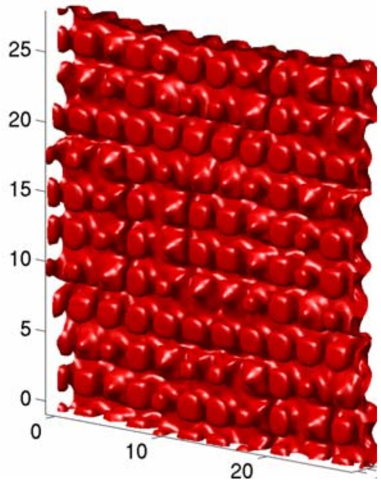

t **= 1 ms**

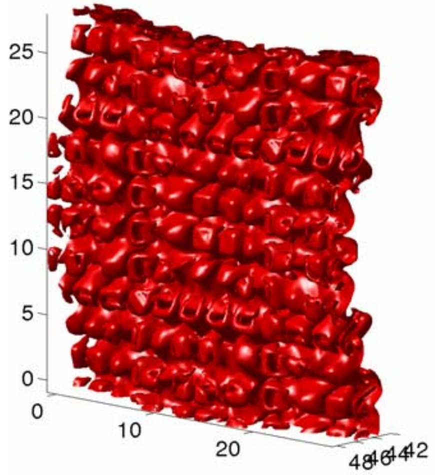

t **= 3 ms**

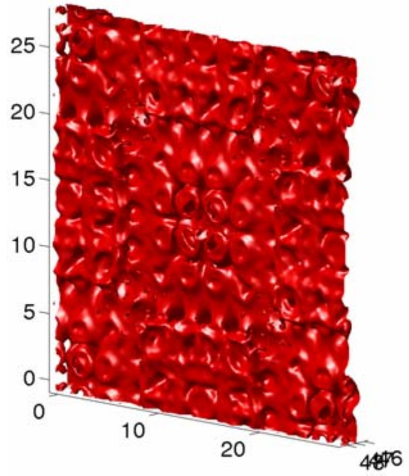

t **= 3.25 ms Reshock**

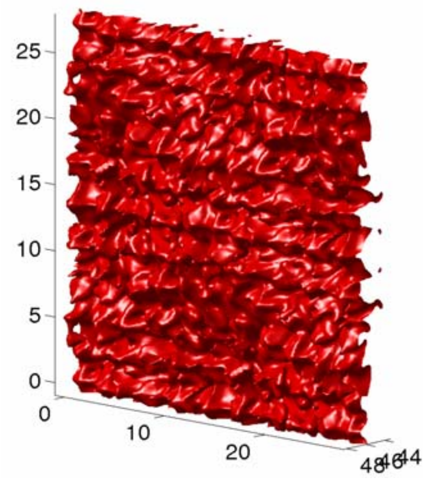

t **= 3.5 ms**

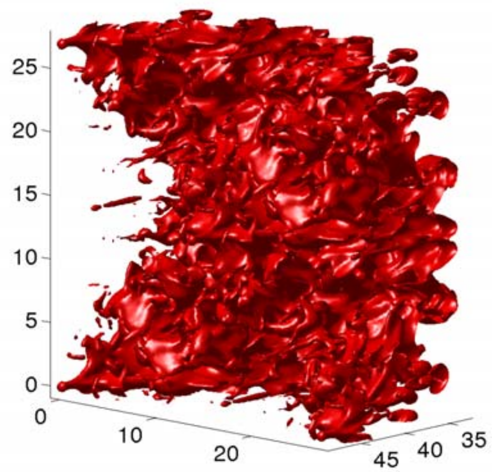

t **= 5 ms**

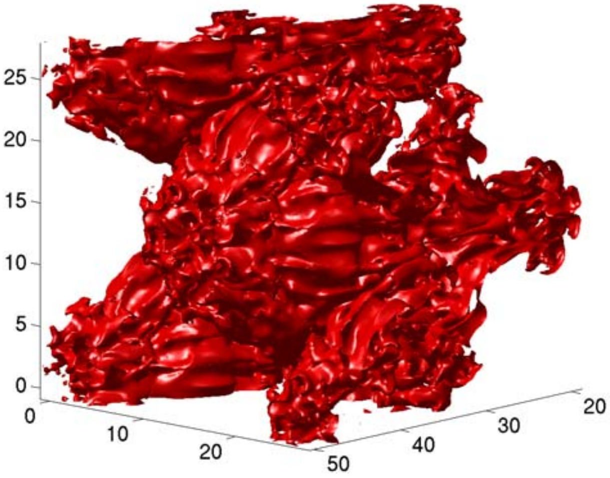

t **= 10 ms**

Mass fraction from 2D simulation shows more coherency and large-scale structure than in 3D

t **= 0 ms**

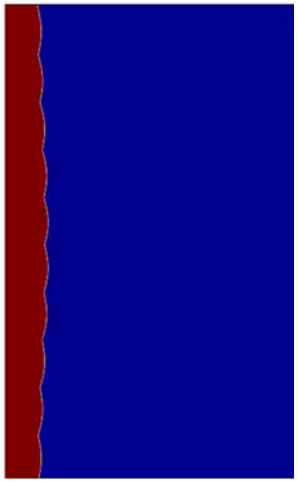

t **= 1 ms**

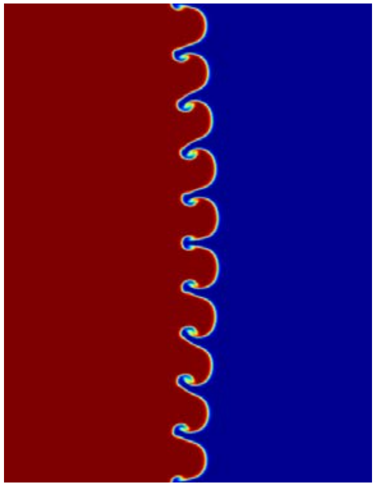

t **= 3 ms**

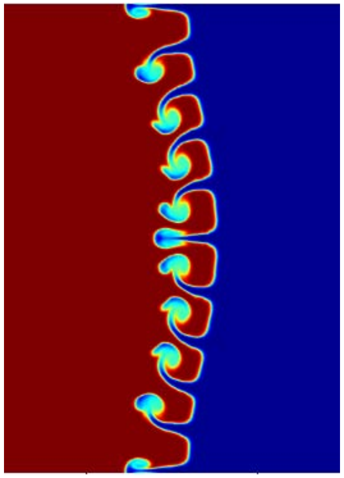

t **= 3.25 ms Reshock**

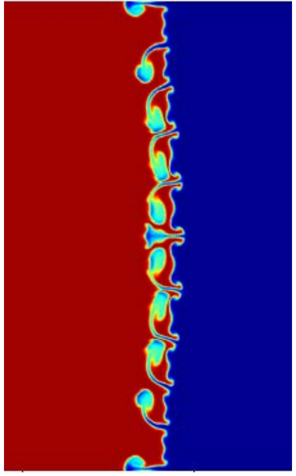

t **= 3.5 ms**

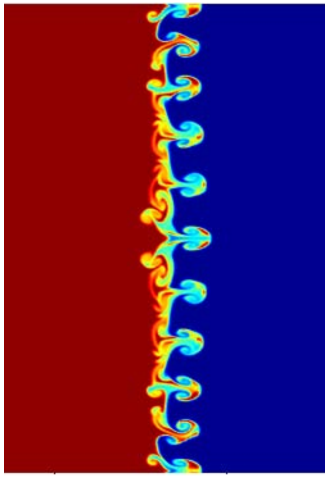

t **= 5 ms**

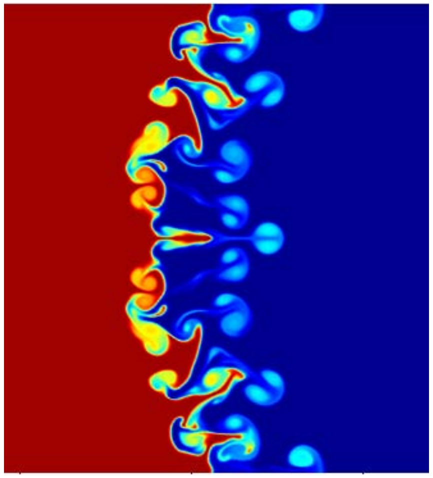

t **= 10 ms**

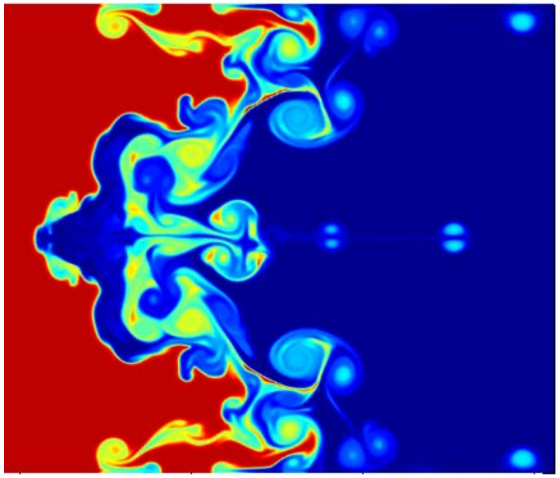

The mixing layer growth is in very good agreement with experimentally-measured growth rate following reshock

- **Amplitude growth also in generally good agreement with Mikaelian reshock model $h(t) = 0.28\, A^{+}\, [u]\, t$**
- **Amplitude growth prior to reshock overestimated**
  - **Limited resolution along shock propagation direction**
  - **Choice of initial perturbation (membrane break-up issues)**
- **2D amplitude growth slightly slower than 3D growth before reshock, and significantly slower after reshock**
- **$da_{3D}/dt > da_{2D}/dt$**

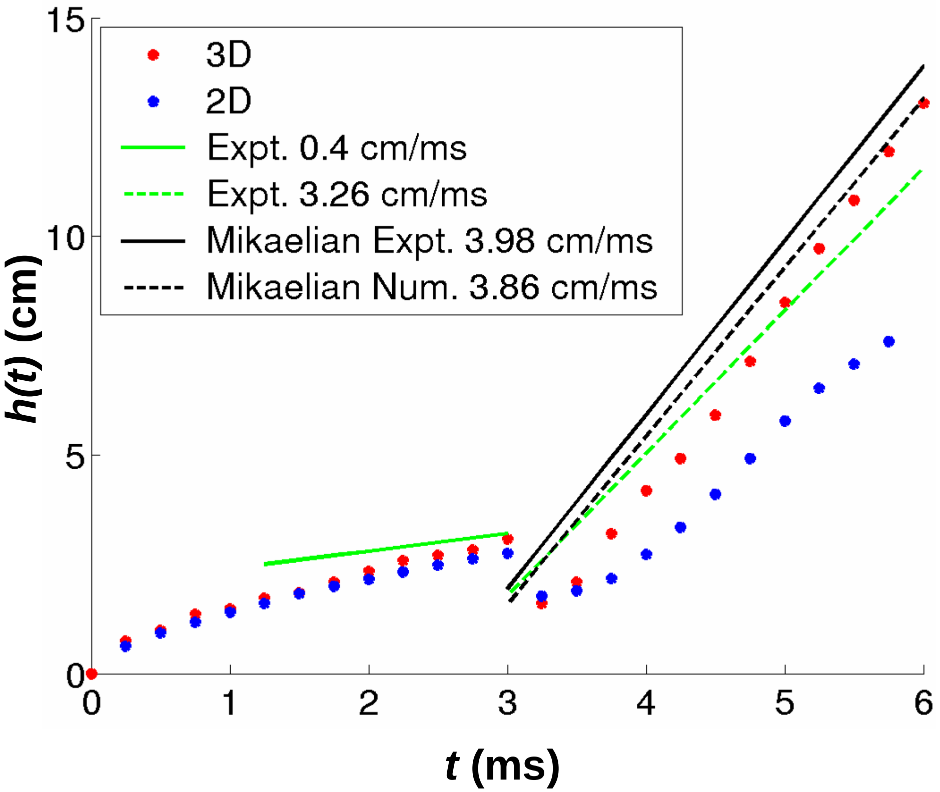

Mole fraction profiles exhibit more spatial structure in two dimensions than in three dimensions

2D WENO 5

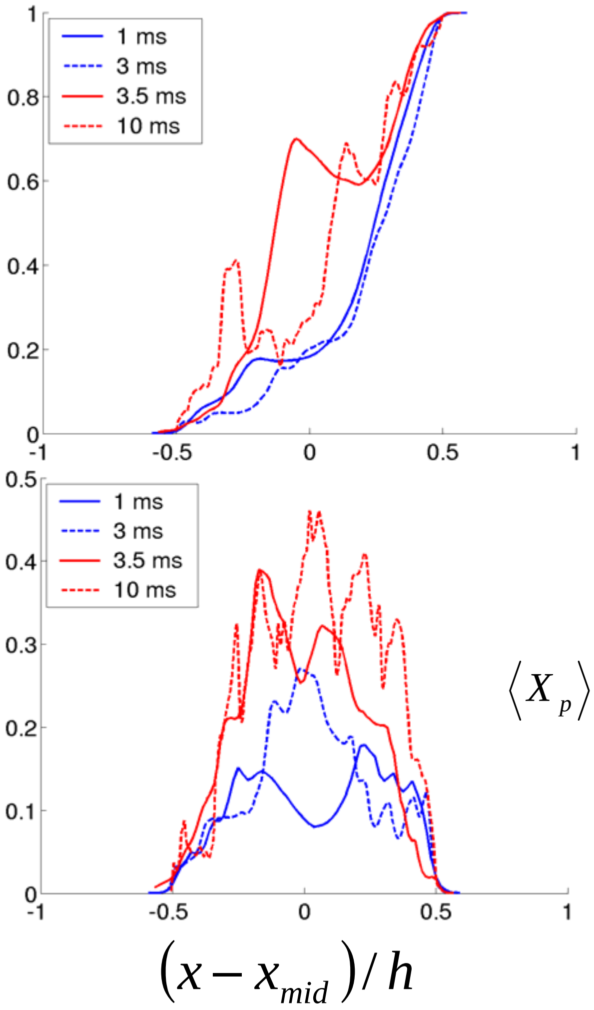

$$\langle X\rangle = \frac{\langle\rho\rangle-\rho_2}{\rho_2-\rho_1}$$

$$\langle X_p\rangle = \begin{cases}\dfrac{\langle X\rangle}{X_s} & \text{for } \langle X\rangle \le X_s = \dfrac{1}{2}\\[2ex] \dfrac{1-\langle X\rangle}{1-X_s} & \text{for } \langle X\rangle > X_s = \dfrac{1}{2}\end{cases}$$

3D WENO 5

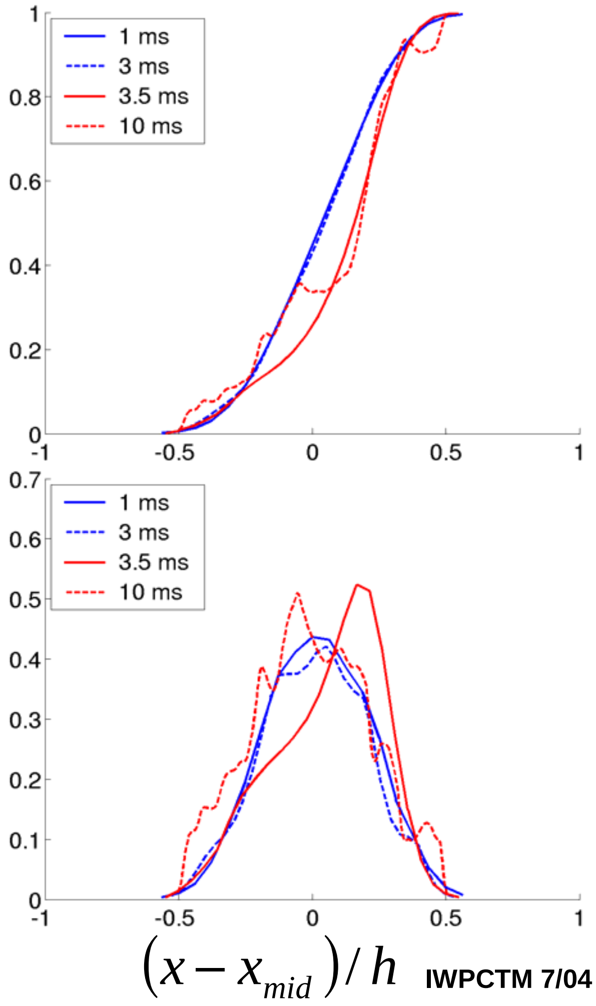

Mixing profile and mixing parameter exhibit different spatial and temporal behavior in 2D and 3D

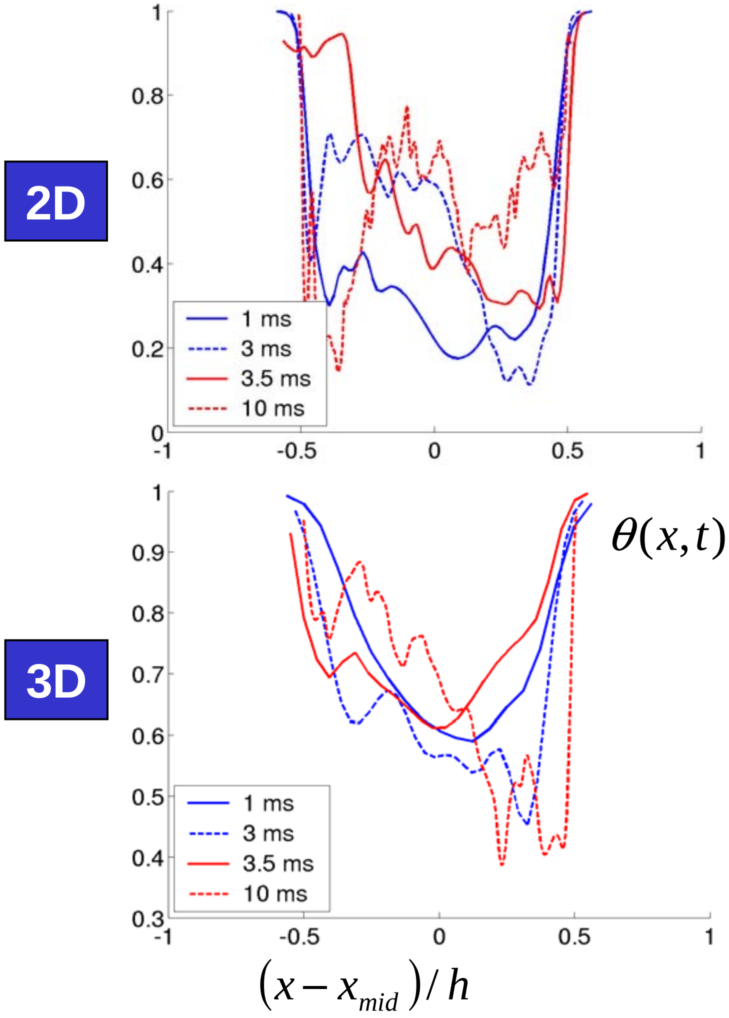

$$\theta(x,t) = \frac{\langle f_1 f_2 \rangle}{\langle f_1 \rangle \langle f_2 \rangle}$$

$$\Theta(t) = \frac{\int_{x\in[h_s,h_b]} \langle f_1 f_2 \rangle d^d x}{\int_{x\in[h_s,h_b]} \langle f_1 \rangle \langle f_2 \rangle d^d x}$$

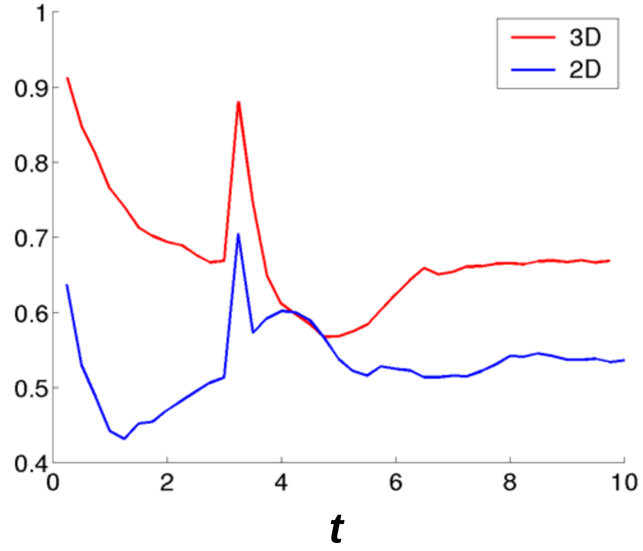

- **$\Theta_{3D} > \Theta_{2D}$ so more overall mixing in 3D**
- **Θ_{3D} and Θ_{2D} differ qualitatively before and after reshock**
- **Both appear to asymptote to different values**

Reshock amplifies the kinetic energy at all scales

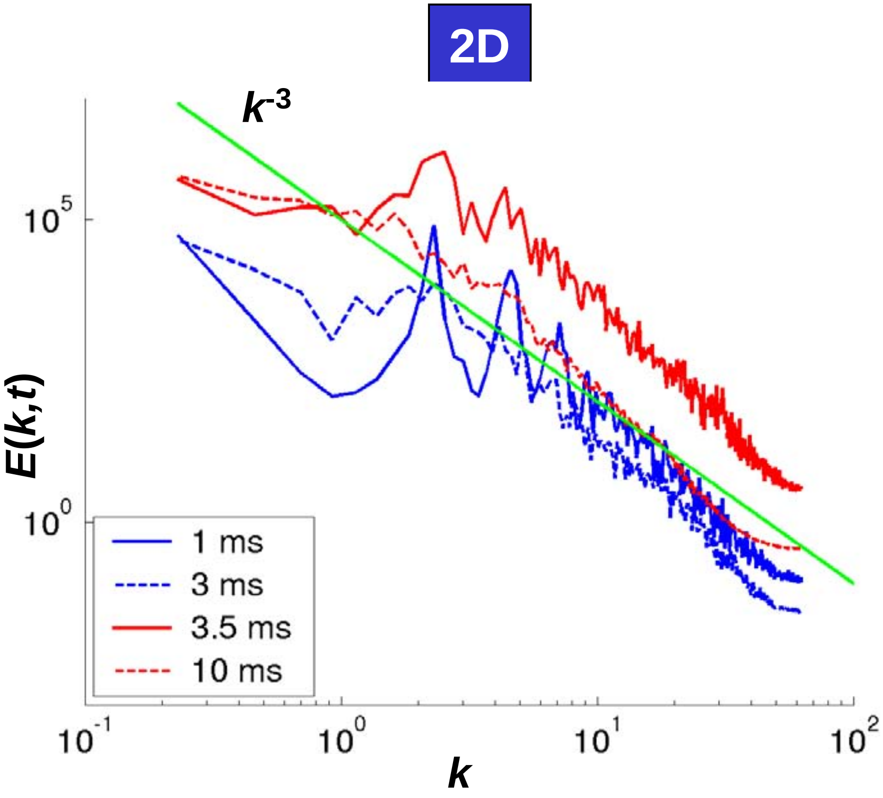

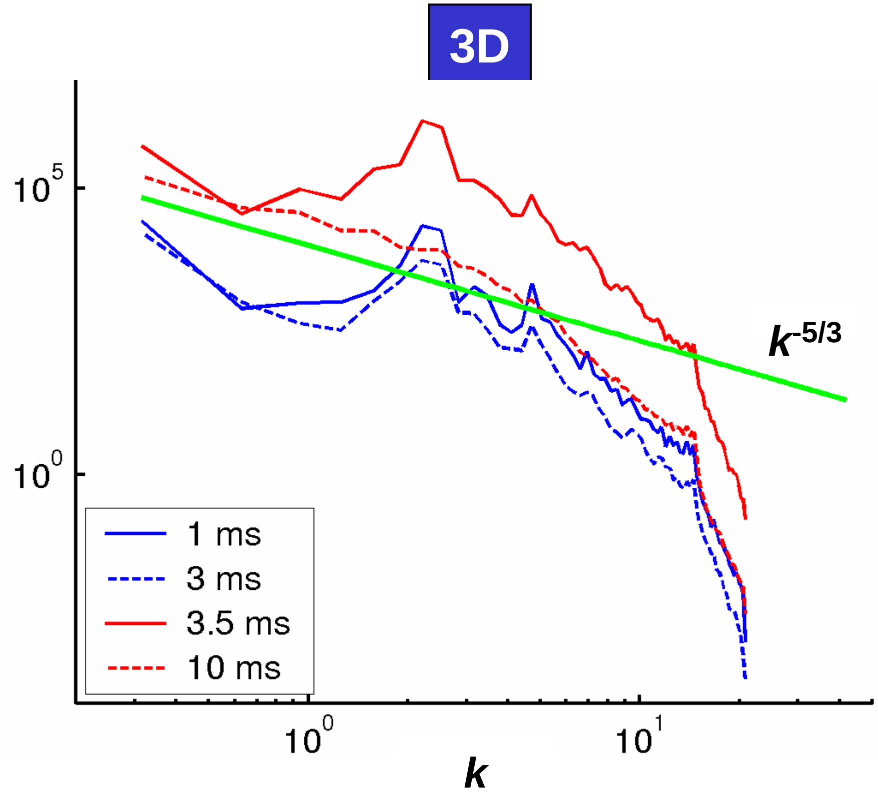

- **Late-time 2D spectrum somewhat steeper than k^{-3}**
- **Late-time 3D spectrum may have a $k^{-5/3}$ large-scale spectrum, with dissipation dominating at intermediate and small scales**

The 401 × 257^2 WENO 5 simulation is too limited in resolution to exhibit a scaling subrange in the 3D kinetic energy spectrum at the mid-slice at *t* = 5 ms

compensated spectrum

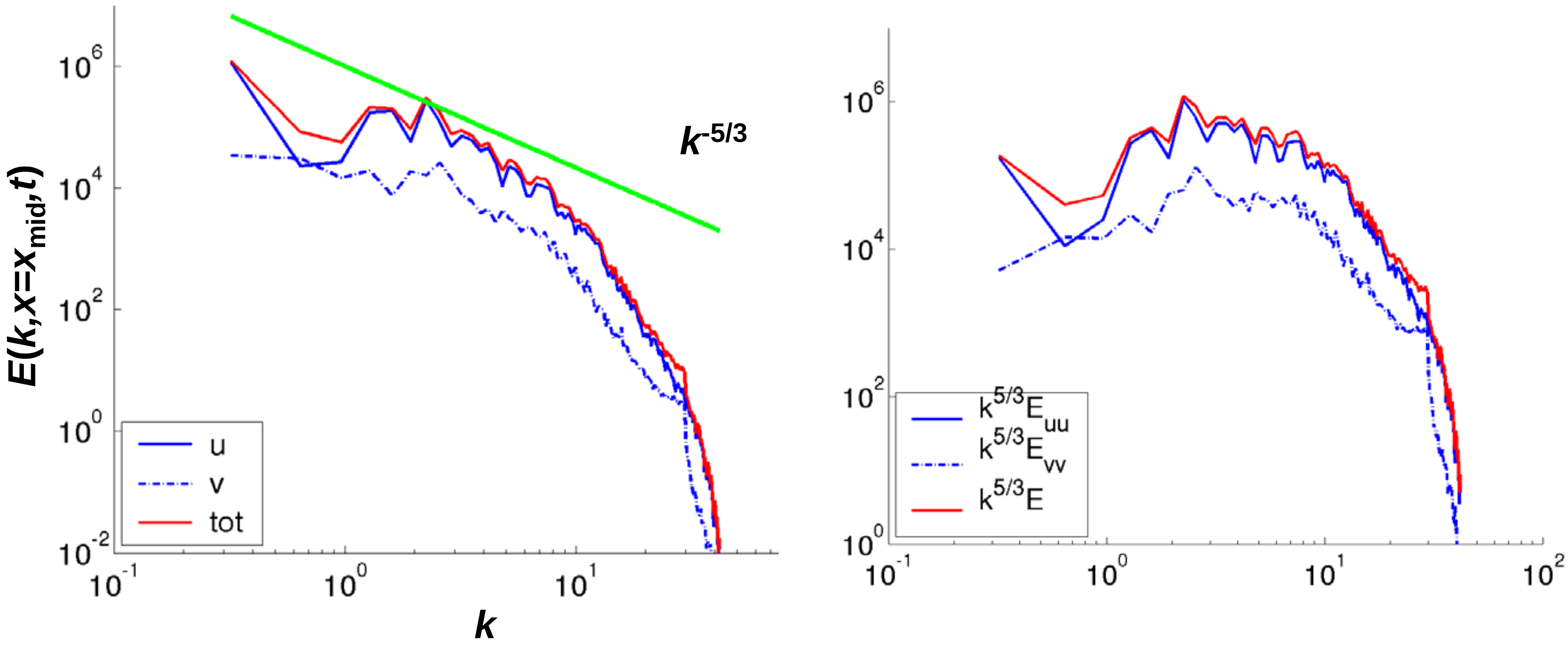

The structure and magnitude of the Reynolds stress components differ considerably in 2D and 3D, acquiring large values after reshock

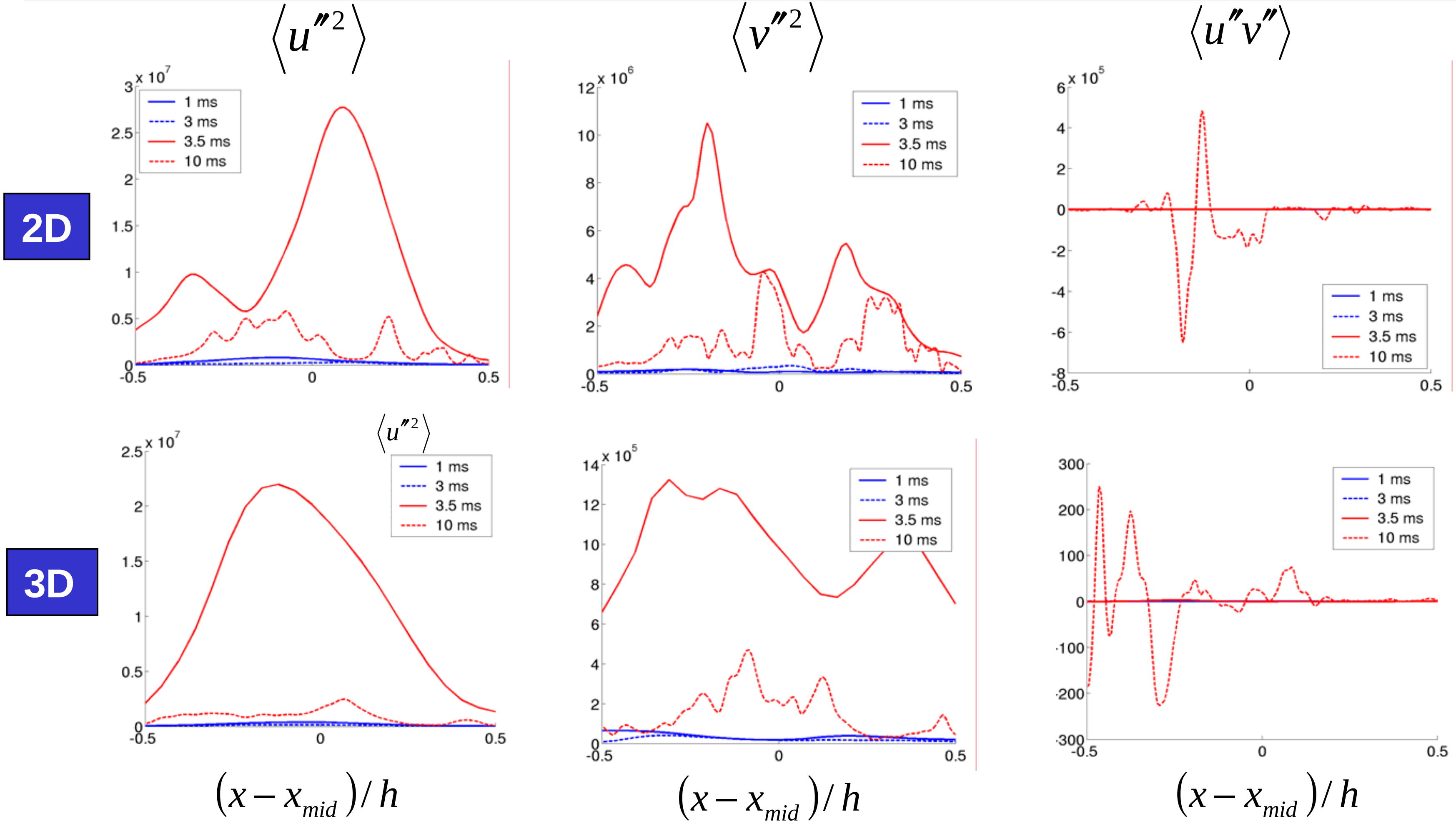

Baroclinic production is the dominant enstrophy generation mechanism in 2D, while baroclinic production and vortex stretching are the dominant mechanisms in 3D

$$\frac{\partial\langle\Omega\rangle}{\partial t} = \left\langle \rho\,\omega_j\,\omega_i\frac{\partial v_j}{\partial x_i}\right\rangle + \left\langle \varepsilon_{ijk}\frac{\omega_i}{\rho}\frac{\partial\rho}{\partial x_j}\frac{\partial p}{\partial x_k}\right\rangle - \left\langle\frac{\partial}{\partial x_j}\left(\Omega v_j\right)\right\rangle - \left\langle 2\rho\Omega\frac{\partial v_i}{\partial x_i}\right\rangle$$

3D

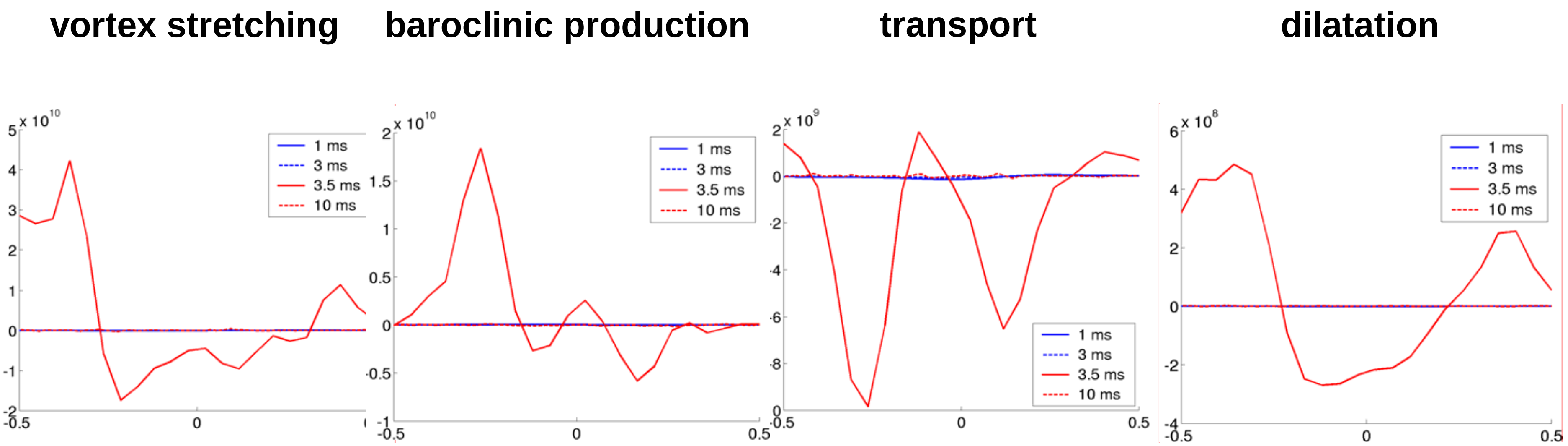
vortex stretching **baroclinic production** **transport** **dilatation**

The buoyancy and Reynolds stress production are dominant mechanisms in 3D, and the pressure-dilatation is also large

$$\frac{\partial}{\partial t}\left\langle \overline{\rho}\, E'' \right\rangle = -\left\langle \overline{\rho v_i'' v_j''}\, \frac{\partial \tilde{v}_i}{\partial x_j} \right\rangle - \left\langle \overline{v_j''}\, \frac{\partial \overline{p}}{\partial x_j} \right\rangle - \left\langle \frac{\partial}{\partial x_j}\left(\overline{\rho}\, E''\, \tilde{v}_j'' \right) \right\rangle + \left\langle \overline{p' \frac{\partial v_i''}{\partial x_i}} \right\rangle - \left\langle \frac{\partial}{\partial x_j}\left(\frac{\overline{\rho v''^2\, \tilde{v}_j''}}{2} \right) \right\rangle - \left\langle \frac{\partial}{\partial x_j}\left(\overline{p' \tilde{v}_j''} \right) \right\rangle$$

3D

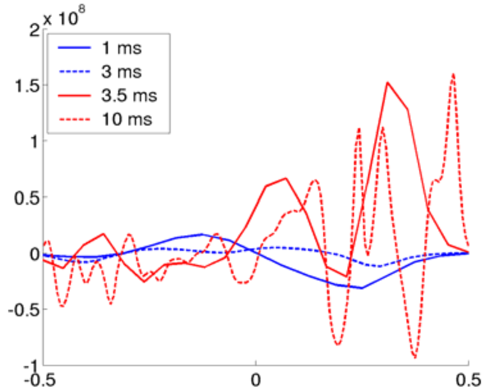

Reynolds stress production

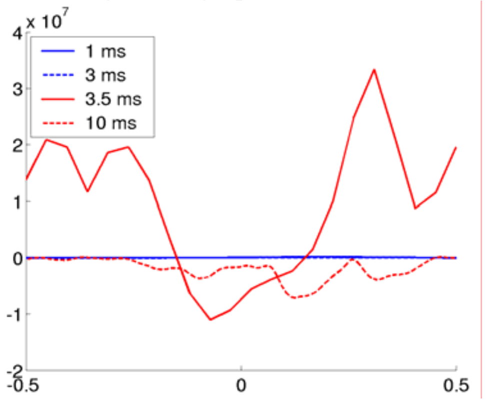

buoyancy production

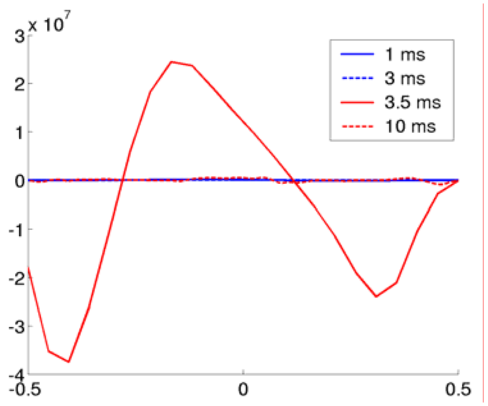

advection

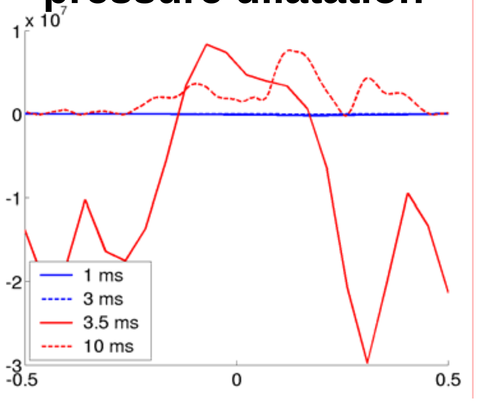

pressure dilatation

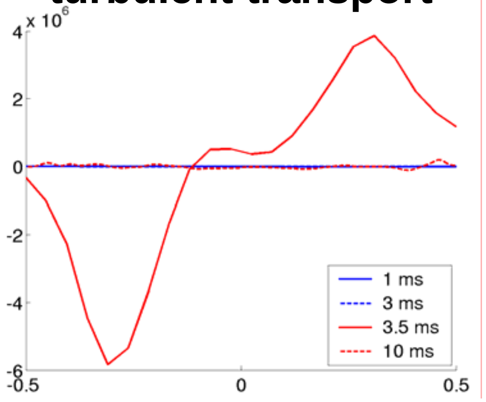

turbulent transport

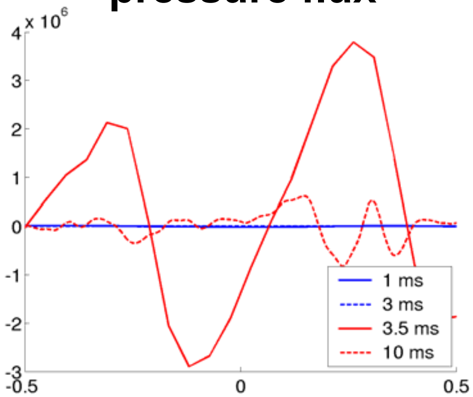

pressure flux

High-resolution simulations provide flow structure, spectra, and statistics of reshocked, multi-mode Richtmyer-Meshkov instability

- **Simulations of *Ma* = 1.5 Vetter-Sturtevant experiment before and after reshock showed dramatic differences in 2D and 3D**
  - **Mixing layer widths grow differently in 2D and 3D**
  - **Structure of mixing profiles and statistics change following reshock and are different in 2D and 3D**
  - **Energy spectra showed that fluctuations are significantly enhanced by vorticity deposition by second shock**
  - **Yet higher resolution needed in 3D to obtain scaling**
  - **Signature of reshock captured in evolution of kinetic energy and enstrophy; nature of fluctuations different in 2D and 3D**
  - **2D and 3D simulations indicate that, following reshock in 3D, vortex stretching and baroclinic production are very important mechanisms**
  - **Reynolds stress and buoyancy production are dominant mechanisms in turbulent kinetic energy transport**